Article

Analysis of scanning electron microscopy images to investigate adsorption processes responsible for detection of cancer biomarkers

Valquiria Cruz Rodrigues, Cesar Comin, Juliana Coatrini Soares, Andrey Coatrini Soares, Matias Eliseo Melendez, José Humberto Tavares Guerreiro Fregnani, André Lopes Carvalho, Luciano da Fontoura Costa, and Osvaldo Novais Oliveira, Jr.

ACS Appl. Mater. Interfaces, **Just Accepted Manuscript** • DOI: 10.1021/acsami.6b16105 • Publication Date (Web): 24 Jan 2017

Analysis of Scanning Electron Microscopy Images to Investigate Adsorption Processes Responsible for Detection of Cancer Biomarkers

Valquiria da Cruz Rodrigues[1*], Cesar Comin[1], Juliana Coatrini Soares[1], Andrey Coatrini Soares[1,2], Matias Eliseo Melendez[3], José Humberto T. G. Fregnani[3], André L. Carvalho[3] Luciano da F. Costa[1], Osvaldo N. Oliveira Jr.[1]

[1]*São Carlos Institute of Physics, University of São Paulo, 13560-970 São Carlos-SP, Brazil*

[2]*Departament of Materials Engineering, São Carlos School of Engineering, University of São Paulo, 13563-120, São Carlos, SP. Brazil*

[3]*Molecular Oncology Research Center, Barretos Cancer Hospital, 14784-400, Barretos-SP, Brazil*

Corresponding author: valbarioto@gmail.com

ABSTRACT

Adsorption processes are responsible for detection of cancer biomarkers in biosensors (and immunosensors), which can be captured with various principles of detection. In this study, we used a biosensor made with nanostructured films of polypyrrole and p53 antibodies, and image analysis of scanning electron microscopy data made it possible to correlate morphological changes of the biosensor with the concentration of cells containing the cancer biomarker p53. The selectivity of the biosensor was proven by distinguishing images obtained with exposure of the biosensor to cells containing the biomarker from those acquired with cells that did not contain it. Detection was confirmed with cyclic voltammetry measurements while the adsorption of the p53 biomarker was probed with polarization-modulated infrared reflection absorption (PM-IRRAS) and a quartz crystal microbalance (QCM). Adsorption is described using the Langmuir-Freundlich model, with saturation taking place at a concentration of 100 Ucells/mL. Taken together, our results point to novel ways to detect biomarkers or any type of analyte for which detection is based on adsorption as is the case of the majority of biosensors.

Keywords: Imunnosensor, p53, Head and Neck Cancer, Langmuir-Freundlich, SEM, Image Processing, Circularity.

INTRODUCTION

The need for early diagnosis of cancer has sparked extensive research into biosensors and immunosensors fabricated with nanostructured films[1], especially because detection of cancer biomarkers in body fluids can potentially be made before

symptoms appear for the disease. A biomarker, or biological marker, is a substance used as an indicator of a biological state. The concentration of a biomarker away from a reference level is an important indicator to diagnose pathogenic processes or a pharmacological response to monitor after a therapeutic intervention.[2] Various detection methods and types of biosensors have been used to detect an equally wide variety of biomarkers[3,4], including electrochemical biosensors[5,6,7]. The performance of these biosensors depends on the way nanomaterials and biomolecules are combined, and therefore control of film architecture is essential, which is normally achieved using techniques such as Langmuir−Blodgett (LB), layer-by-layer (LbL) and self-assembled monolayers (SAMs).[8–10] The concept of nanoarchitectonics has been introduced because biosensors must be designed in order to minimize denaturing of the biomolecules and enhance the sensitivity and selectivity. A common feature in these biosensors is that their selectivity is ascribed to the presence of very specific interactions between the biomolecule immobilized in the biosensor, such as an antibody or antigen, and the analyte – which would be the corresponding antigen or antibody. With such interactions, the biosensing mechanism is essentially a specific, irreversible adsorption of the analyte on the biosensor surface[5]. Hence, investigation of adsorption processes may be a generic avenue for the design and characterization of biosensors.

In this work, we study the adsorption processes behind biosensing with image analysis of scanning electron microscopy data. We chose the biomarker p53 as a testbed for proof-of-principle experiments owing to its importance since the major genetic alteration in human cancers is mutation of the p53 tumor suppressor gene, present in about 50% of the tumors[11,12]. The *TP53* gene is located on the short arm of human chromosome 17, whose function is to encode the synthesis of a nuclear phosphoprotein

of 53 kD which contains 393 amino acids expressed at basal levels in all normal cells[13]. This protein has the ability to bind to specific DNA sequences, being a transcription factor that controls positively or negatively the expression of several genes in cellular pathways[14]. Mutation and inactivation of the p53 gene are associated with cancer because of an increased cell population with higher genetic instability[15]. An example of p53 mutation occurs in dietary intake of aflatoxin which can result in liver cancer, characterized by the AGG to AGT transversion mutation (underlined) at codon 249, which promotes the replacement of an arginine with a serine[16]. Another example would be exposure to benzopyrene, powerful carciogenic and mutagen found in cigarette and related to lung cancer[17].

Detection of p53 has been made mainly with immune histochemical tests[14,18] and enzyme-linked immunoassays[14,19,20]. Here we use nanostructured films of polypyrrole and anti-p53 antibodies for detecting p53 with different methods. In addition to demonstrating that image analysis can be used to determine the p53 concentration, we complement the study with a quartz crystal balance and polarization-modulated infrared reflection absorption spectroscopy (PM-IRRAS) to investigate the adsorption mechanisms. Furthermore, we verify that detection can also be made with standard cyclic voltammetry.

METHODS

The anti-p53 monoclonal antibody and polypyrrole were purchased from Dako (clone DO-7) and Sigma Aldrich, respectively. Breast cancer MCF7 (expressing the p53 antigen and referred to as positive cells) and osteosarcoma Saos-2 cells (negative for the

p53 protein expression) were obtained from American Tissue Culture Collection (ATCC) and cultured at the Barretos Cancer Hospital (Barretos, São Paulo, Brazil). Whole cell lisates were obtained by three cycles of freeze-thaw and stored at -80°C. The biosensor was produced by coating in commercial printed electrode carbon with 4mm diameter working electrode (Dropsens, Spain) with a one-bilayer LbL film made with polypyrrole and anti-p53 antibodies. The $5mm^2$ carbon electrode was immersed into polypyrrole solution 5 wt % dispersion in H_2O**,** for 15 min, washed with copious amounts of Milli-Q water, and dried under nitrogen. The layer of p53 antibody in PBS buffer was then adsorbed with a soaking time of 30 min.

Deposited films on an aluminum support and covered with a thin layer of carbon for electrical contact and image generation were characterized with a scanning electron microscope (DSM 960 Zeiss, Germany). The carbon thin layer was used to maintain electrical contact. After coating, the samples were placed in a vacuum chamber to remove moisture. For atomic force microscopy (AFM), a Nanoscope Digital IIIA instrument was used in the tapping mode for films deposited on carbon electrodes. A quartz crystal microbalance (QCM 200) (Stanford Research System Inc) was used to determine the amount of mass deposited during the detection process, with the LbL film deposited on gold-coated piezoelectric quartz crystal. Cyclic voltammetry was employed to detect the biomarker in a potential range between -0.6 and 0.6V. The current was monitored as a function of biomarker concentration ranging from 0.01 to 1000 $Ucell.mL^{-1}$.

An image processing approach was employed to quantify the “roughness” of the samples of SEM images. First, a Gaussian smoothing filter[21] with a standard deviation of 6 nm was applied to the images. Then, an adaptive thresholding technique[21] was used

for image binarization. More specifically, the intensity value, I_i, of each image pixel, i, was compared to the average intensity value, $\bar{I}_{Ri}$, calculated over all pixels inside a disk of radius 300 nm centered at pixel i. Whenever $I_i > \bar{I}_{Ri} + T$, the pixel i receives value '1' in the resulting binary image (and '0' otherwise). The threshold parameter T sets the relative intensity required for the pixel, compared to its neighborhood. Here, we considered $T = 3$. The resulting binary image contains what we call *objects*[22], defined as sets of adjacent white pixels (with value '1'). Objects smaller than 700 nm^2 were eliminated, since they are likely caused by noise. The final binary image was used for sample characterization.

A systematic procedure was adopted to determine which features on the images could be indicative of adsorption of the analyte molecules (in our case p53 antigens), since one should expect the film morphology to be affected by such adsorption. In particular, we used a feature selection method to obtain the metric that most explained the differences in the images when the p53 concentration was varied. Among the metrics tested, namely circularity, area, lacunarity, intensity and Fourier descriptors, we found that circularity[23] of each object on the image was the most promising. The circularity of object b is defined as $C_b = 4\pi A_b / P_b^2$, where A_b is the object area and P_b is its perimeter. This measure quantifies how similar object b is to a circle. That is, if the object is a perfect circle, $C_b = 1$. If the object has a tortuous shape or rough borders, its squared perimeter will be larger than $4\pi A_b$, and therefore $C_b < 1$. In order to characterize each image, the average and standard deviation of the objects circularity were calculated (Fig.1).

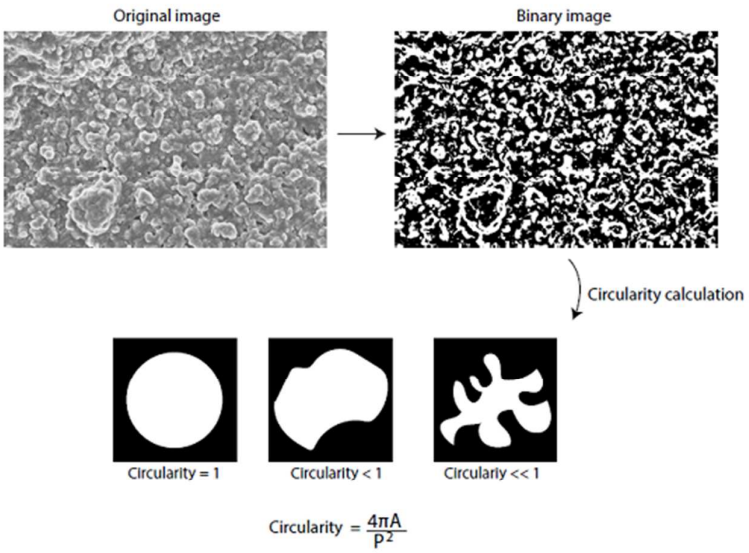

Figure 1. Methodology used for circularity calculation. The original image is transformed into a binary one. The circularity of each white object is then quantified. Objects that are similar to disks have a circularity close to 1, while more irregular objects are represented by smaller circularity values.

RESULTS AND DISCUSSION

There is growing evidence in the literature[5,7] that adsorption is responsible for the detection mechanism in many biosensors, such as those based on antigen-antibody interactions (also referred to as immunosensors). This is proven here with measurements with a quartz crystal microbalance (QCM), and Fig. 2 shows an increasing mass adsorbed onto the electrode with increasing concentration of antigen-containing cells (positive cells). In contrast, there was practically no increase in mass when the electrode was exposed to negative cells, thus demonstrating the absence of non-specific adsorption. The adsorption isotherm in Fig. 2 can be fitted with the Langmuir-Freundlich model, as indicated by the full line in the figure.

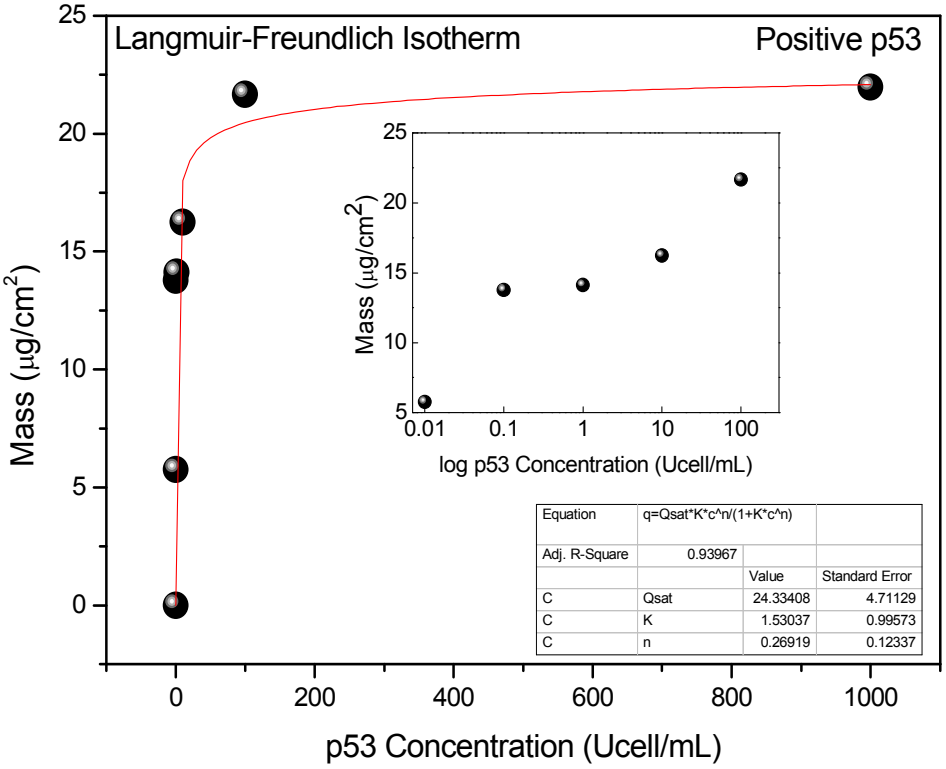

Figure 2. Adsorption isotherm obtained with a QCM, in which the mass adsorbed during the biosensing experiment is plotted against the concentration of p53 antigen. The solid curve shows the fitting with the Langmuir-Freundlich model. The insert shows the data in logarithmic scale.

That adsorption during biosensing experiments is related to the antigen p53 can be confirmed with the PM-IRRAS spectra in Fig. 3, whose main bands are listed in Table 1. Changes in the spectra are caused by deposition of the distinct layers of the biosensor and by adsorption of p53, having the spectrum of the Au substrate as the reference. With deposition of PPY, the spectrum (black line) shows characteristic bands of polypyrrole at 1460 cm^{-1} (C-C symmetric ring stretching), 1534 cm^{-1} (C-N asymmetric ring stretching) and 1600 cm^{-1} (C=C).[24,25] When the anti-p53 antibodies (AB) were adsorbed onto the PPY film (red line), the 1652 cm^{-1} band increased due to carbonyl

groups (C=O) of adsorbed AB[26]. PPY bands also appear between 1500-1612 cm^{-1}, and significant differences are observed at higher energy regions with appearance of the CH_2 band (in plane bending) at 1433 cm^{-1} and amide II band (N-H out of plane) at 1486 cm^{-1} [27,28]. The antibody-antigen interaction is observed through three large bands at 1446 cm^{-1}, 1540 cm^{-1} and 1650 cm^{-1}, associated, respectively, with the CH_2 group, amide II (N-H out of plane) and amide I (C=O stretching)[26,28,29]. Indeed, this interaction is best observed in the amide I region, with a slight shift in the band (from 1652 cm^{-1} to 1650 cm^{-1}), and an increase in the area of C=O band, present in both AB and p53 (AG) molecules[26,29].

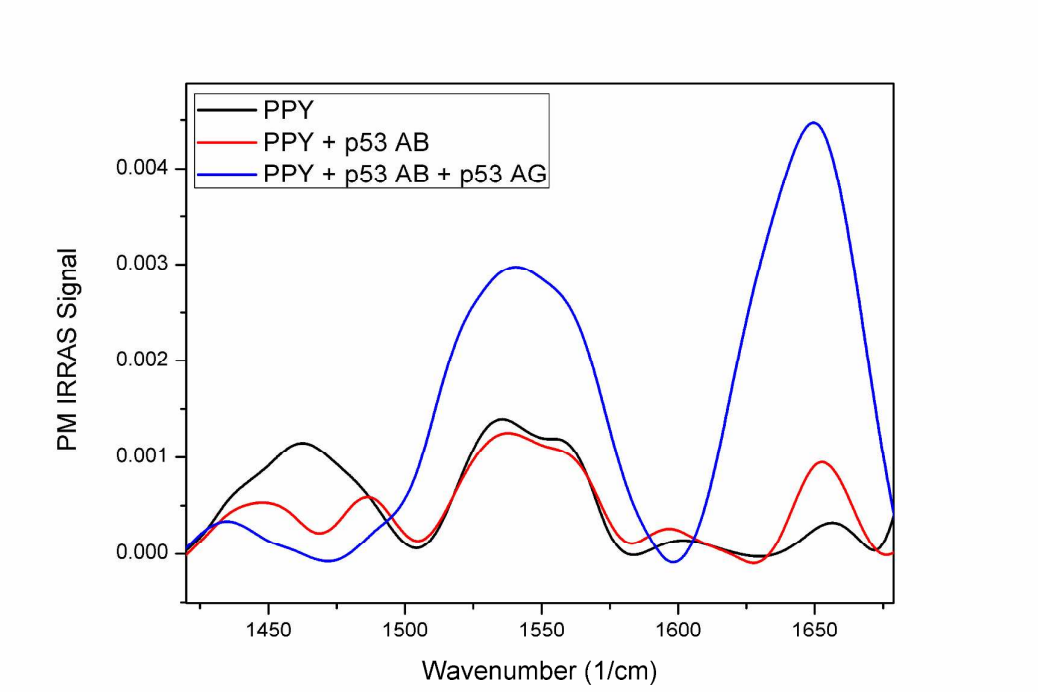

Figure 3. PM-IRRAS spectra of a PPY layer (black), coated with a layer of p53 antibodies (PPY/p53 AB, red) and after adsorption of p53 antigens (PPY/p53 AB/AG, blue). The spectrum of the gold support was used as reference, which was subtracted

from the spectra of the films. The term PM-IRRAS signal is used as it refers to the difference in reflectivities between *s* and *p* polarizations.

Table 1 - Absorption bands in the PM-IRRAS spectra

Group	**Wavenumber (cm^{-1})**
CH2 (in plane bend) (AB; AG)	1433; 1446
C-C symmetric ring stretching (PPY)	1460
Amide II (AB) (N-H out of plane)	1486
C-N asymmetric Ring Stretching (PPY)	1534; 1538
amide II (AG) (N-H out of plane)	1540
C=C (ppy)	1600
amide I (AG) (C=O stretching)	1650
amide I (AB) (C=O stretching)	1652

Having confirmed that adsorption takes place when the biosensor is exposed to the antigen p53, we tested the hypothesis of using changes in film morphology as a principle of detection. SEM images such as those of Fig. 4 were processed in an attempt to identify differences in morphology induced by exposure to p53. The morphology and chemical composition of the biosensor, studied using elemental analysis by EDX, are given in Fig. S1 in the Supplementary Information.

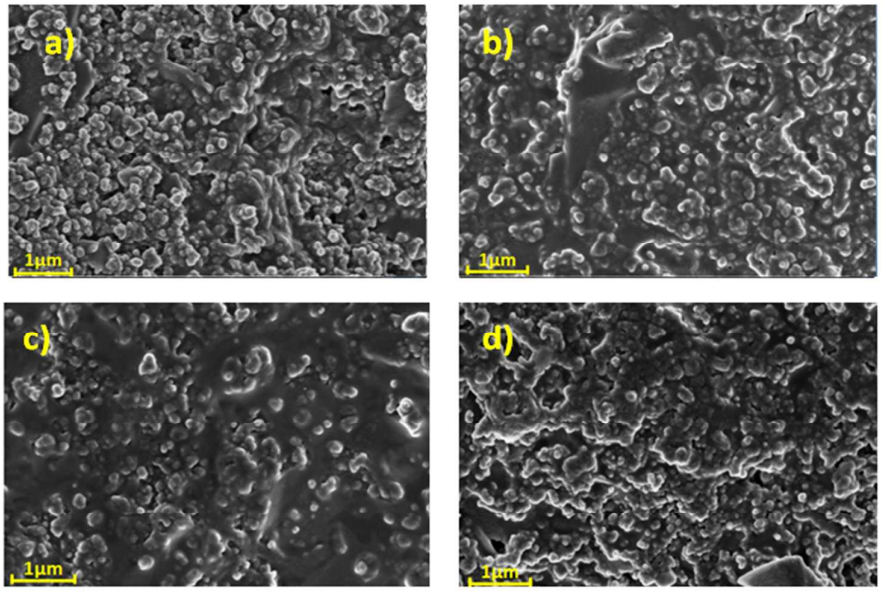

Figure 4. SEM images with increase of 50.000x of films: a) PPy, b) PPy/anti p53, before exposure to the antigen p53, c) PPy/anti p53, after exposure to the antigen p53 and d) PPy/anti p53, after exposure to the antigen p53 at saturation (i.e. very high concentration).

The most efficient way to distinguish between similar images is to quantify salient features, which are normally related to the shape and density of objects identified on the images. Because the distribution of size and shape of objects tends to be non-uniform, useful properties may also be obtained from the standard deviation of the measurements considered. For the microscopy images analyzed here, we found that circularity of the objects was not a distinctive feature of the samples. That is to say, when images were taken from biosensors exposed to different concentrations of the biomarker, the difference in average circularity of the objects was not large. In contrast,

the standard deviation of the circularity varied consistently with the antigen concentration, as shown in Fig. 5. Furthermore, this analysis is consistent with the selectivity of the biosensor, since the standard deviation for non-specific analytes, *viz.* the HCV antigen for hepatitis and cells that did not contain p53 (referred to as p53 negative), was similar to that of the PPy/anti p53 film, before exposure to the antigen p53.

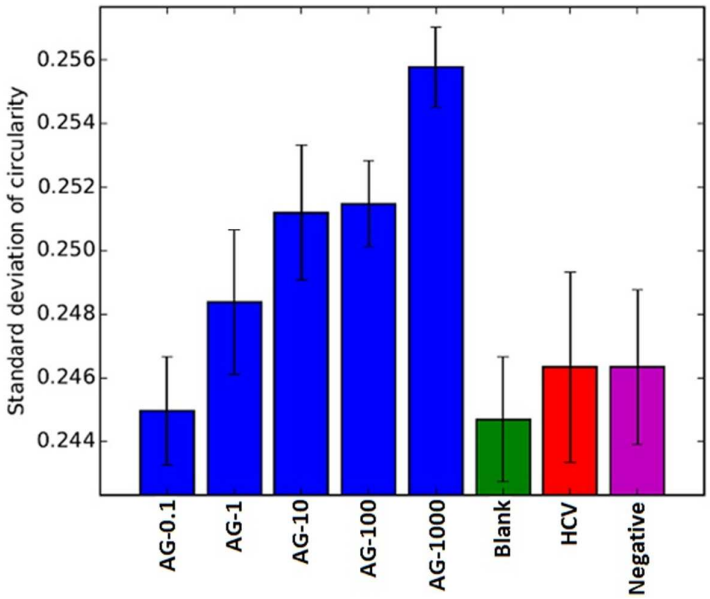

Figure 5. The standard deviation of average circularity obtained in the SEM images varied with the concentration of the antigen p53 to which the biosensor was exposed. Significantly, when non-specific analytes were used, *viz.* for HCV (red), cells that did not contain p53 (negative, magenta), the standard deviation was very similar to that of the PPy/anti p53 film, before exposure to the antigen p53 (green).

We performed subsidiary experiments with AFM to further verify that changes in biosensor film morphology were associated with sensing the antigen p53. Figure S2 in the Supplementary Information shows that the film roughness decreased with p53

concentration until it saturated when all the adsorption sites were occupied. Above this saturation concentration, film roughness increased as there was accumulation of p53, probably with less specific interaction. The latter is consistent with the change in the voltammetric signal discussed below.

We wished to confirm the biosensing performance with a standard method, for which we resorted to cyclic voltammetry. The results are shown in Fig. 6 for PPy/p53 films in 0.1 mol L^{-1} solution of PBS buffer, pH 7.4. A peak is observed around 0.02 mV, which increases and shifts to higher potentials for increasing p53 antigen concentrations up to 10 Ucel/mL. For higher p53 concentrations, the peak tends to return to lower potentials. This response is related to the antibody/antigen interaction, which corroborates AFM results in that the roughening of the film starts to increase for higher concentrations. Therefore, the antibody active sites were all occupied, and thus antigen molecules at higher concentrations may stay on the film surface, making it more resistive and rougher.

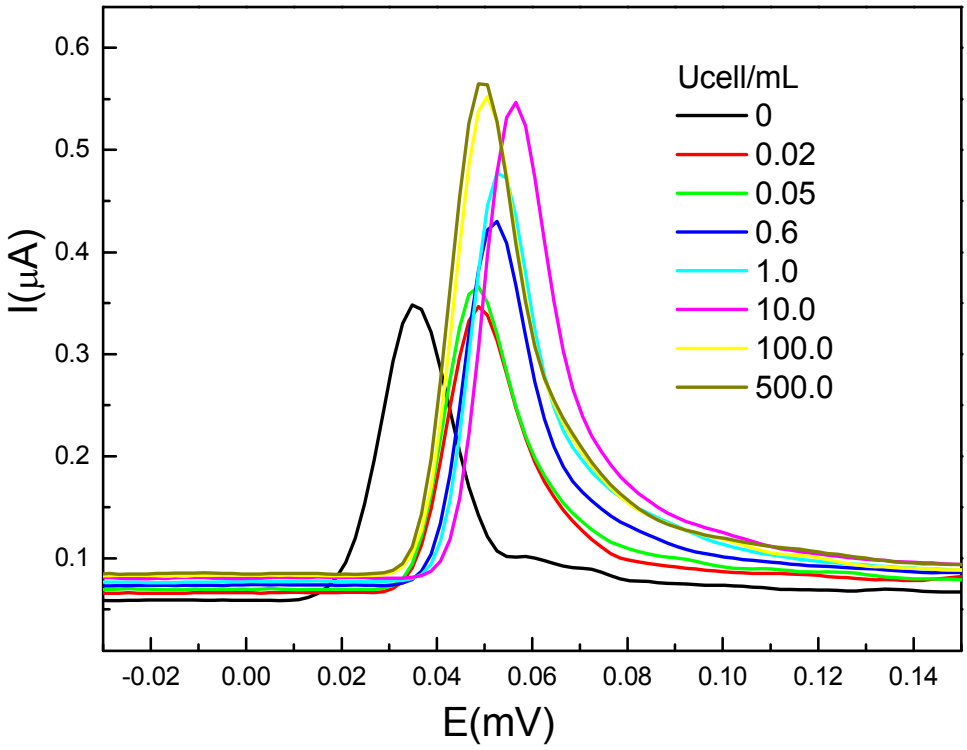

Figure 6. Cyclic voltammetry of PPI/p53 films, in the potential range between -0.6 V and 0.6V vs. SCE in buffer PBS pH 7.4 with p53 antigen ranging between 0 and 500 Ucell/mL.

The concentration dependence was analyzed in two different ways. The peak current varied with p53 concentration as in Fig. 7, which could be fitted with a Langmuir-Freundlich isotherm, as was done for mass adsorption in Fig. 1. At low concentrations, this dependence can be approximated with a linear graph, shown in the inset, from which the sensitivity of the biosensor could be determined as being 1.4×10^{-7} A/UcelmL^{-1}, with 0.6 Ucell/mL as limit of detection. The detection limit was calculated using IUPAC method (LOD = 3SB/S), where SB is the standard deviation of 10 measurements taken from the signal obtained from the blank (a solution identical to that analysed but without the analyte) and S is the slope of the calibration curve (sensitivity of the analytical method[5,30,31]. A value close to that obtained in the ELISA test was

obtained for the detection limit, i.e. 0.5 Ucell/mL[30], thus indicating that the film architecture in the biosensor (PPy/anti p53) is suitable for detecting p53 with high performance. We also observed that a Langmuir-Freundlich isotherm can explain the data for the area in the voltammograms (rather than the peak current), as shown in Fig. S3 in the Supplementary Information. Furthermore, the selectivity of the biosensor was confirmed by verifying the negligible changes in area in Fig. S4 when the biosensor was exposed to non-specific analytes such as HCV, p24, negative p53 and only buffer.

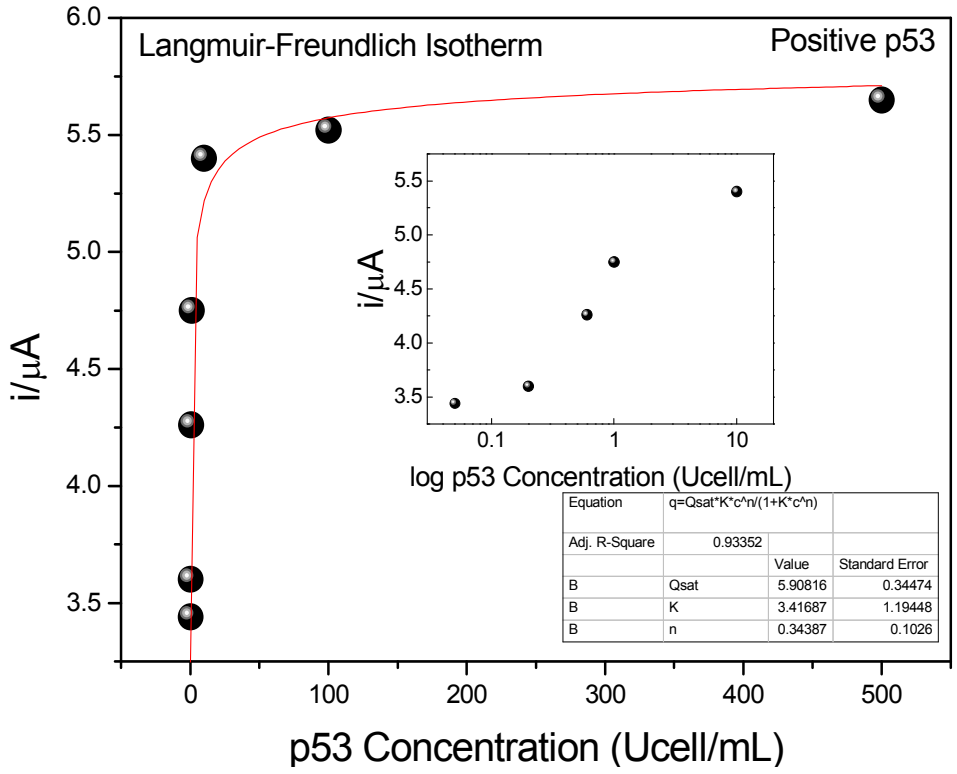

Figure 7. Peak current of cyclic voltammograms for PPY/p53 of Figure 6 for different antigen p53 concentrations.

CONCLUSION AND PERSPECTIVES

Here we investigated in detail the adsorption mechanisms responsible for detection of the cancer biomarker antigen p53, which was made to interact with an LbL film containing a semiconducting polymer and a layer of the anti-p53 antibodies. Antibody-antigen interactions could be identified from the changes in the PM-IRRAS spectra, which were also used to monitor film growth in biosensor fabrication. Adsorption measured with a crystal quartz microbalance and inferred from cyclic voltammetry measurements could be explained with a Langmuir-Freundlich model, as it was observed in detecting a biomarker for head and neck cancer[5]. These cyclic voltammetry experiments were useful to demonstrate that the LbL film was efficient for detecting p53 with high performance, with limit of detection of 0.6 Ucell/mL, similar to the ELISA method, and with good selectivity.

In order to explore the nature of the biosensing mechanism, based on adsorption, we tested the hypothesis of possible detection using image analysis of SEM images taken with the biosensor before and after exposure to p53. Indeed, we showed that the standard deviation of the circularity of objects on the image can be correlated with the concentration of p53. Selectivity was also demonstrated as the standard deviation of circularity was practically the same for images taken after exposure of the biosensor to non-specific analytes. Using image analysis for detecting biomarkers with nanostructured biosensors appears rather unusual, but may represent a new avenue for obtaining easy-to-use diagnostic methods that do not require intervention of experts. In the proof-of-principle demonstration in this study we used SEM images, which are obviously non trivial to acquire and are not amenable to be used in common practice by medical doctors. We shall nevertheless pursue this idea by verifying whether similar performance can be achieved with other types of microscopy. In an ideal scenario,

optical microscopy could be used through a smartphone[32,33,34], which would make it possible to use a single instrument (smartphone) for the whole process of recording the biosensing procedure and treating the data through image analysis. It remains to be seen whether features of the adsorption process can be captured with lower resolution microscopies, such as optical microscopy.

Acknowledgments

This work was supported by FAPESP (2013/14262-7), CNPq (164613/2014-5) and CAPES (Brazil). CHC thanks FAPESP (2011/22639-8) for financial support. LdFC thanks CNPq (307333/2013-2), NAP-PRP-USP and FAPESP (2011/50761-2) for support.

REFERENCES

(1) Chikkaveeraiah, B. V.; Bhirde, A. A.; Morgan, N. Y.; Eden, H. S.; Chen, X. Electrochemical Immunosensors for Detection of Cancer Protein Biomarkers. *ACS Nano* **2012**, *6* (8), 6546–6561.

(2) Sana, M.; Irshad, S. Research In Cancer and Tumor. *Rev. Breast Cancer Biomark. BRCA1 BRCA2* **2012**, *1*, 1–4.

(3) Bohunicky, B.; Mousa, S. Biosensors: The New Wave in Cancer Diagnosis. *Nanotechnol. Sci. Appl.* **2010**, *4*, 1–10.

(4) Soares, A. C.; Soares, J. C.; Shimizu, F. M.; Melendez, M. E.; Carvalho, A. L.; Oliveira, O. N. Controlled Film Architectures to Detect a Biomarker for Pancreatic Cancer Using Impedance Spectroscopy. *ACS Appl. Mater. Interfaces* **2015**, *7* (46), 25930–25937.

(5) Soares, J. C.; Soares, A. C.; Pereira, P. A. R.; Rodrigues, V. da C.; Shimizu, F. M.; Melendez, M. E.; Scapulatempo Neto, C.; Carvalho, A. L.; Leite, F. L.; Machado, S. A. S.; Oliveira, O. N. Adsorption according to the Langmuir–Freundlich Model Is the Detection Mechanism of the Antigen p53 for Early Diagnosis of Cancer. *Phys Chem Chem Phys* **2016**, *18* (12), 8412–8418.

(6) Moraes, M. L.; Rodrigues, V. C.; Soares, J. C.; Ferreira, M.; de Souza, N. C.; Oliveira, O. N. Immunosensor for HIV-1 Diagnostics Based on Immobilization of the Antigenic Peptide p24-3 Into Liposomes. *J. Nanosci. Nanotechnol.* **2014**, *14* (9), 6638–6645.

(7) Cerrutti, B. M.; Moraes, M. L.; Pulcinelli, S. H.; Santilli, C. V. Lignin as Immobilization Matrix for HIV p17 Peptide Used in Immunosensing. *Biosens. Bioelectron.* **2015**, *71*, 420–426.

(8) Soares, J. C.; Shimizu, F. M.; Soares, A. C.; Caseli, L.; Ferreira, J.; Oliveira, O. N. Supramolecular Control in Nanostructured Film Architectures for Detecting Breast Cancer. *ACS Appl. Mater. Interfaces* **2015**, *7* (22), 11833–11841.

(9) Ariga, K.; Yamauchi, Y.; Rydzek, G.; Ji, Q.; Yonamine, Y.; Wu, K. C.-W.; Hill, J. P. Layer-by-Layer Nanoarchitectonics: Invention, Innovation, and Evolution. *Chem. Lett.* **2014**, *43* (1), 36–68.

(10) Rydzek, G.; Ji, Q.; Li, M.; Schaaf, P.; Hill, J. P.; Boulmedais, F.; Ariga, K. Electrochemical Nanoarchitectonics and Layer-by-Layer Assembly: From Basics to Future. *Nano Today* **2015**, *10* (2), 138–167.

(11) Hamidi-Asl, E.; Raoof, J. B.; Hejazi, M. S.; Sharifi, S.; Golabi, S. M.; Palchetti, I.; Mascini, M. A Genosensor for Point Mutation Detection of P53 Gene PCR Product Using Magnetic Particles. *Electroanalysis* **2015**, *27* (6), 1378–1386.

(12) Chai, Y.; Peng, B.; Dai, L.; Qian, W.; Zhang, Y.; Zhang, J.-Y. Autoantibodies Response to MDM2 and p53 in the Immunodiagnosis of Esophageal Squamous Cell Carcinoma. *Scand. J. Immunol.* **2014**, *80* (5), 362–368.

(13) Levine, A. J.; Momand, J.; Finlay, C. A. The p53 Tumour Suppressor Gene. *Nature* **1991**, *351* (6326), 453–456.

(14) Klumb, C. E.; Cavalcanti Júnior, G. B. Avaliação Dos Métodos de Detecção Das Alterações Do Gene E Proteína P53 Nas Neoplasias Linfóides. *Rev. Bras. Hematol. E Hemoter.* **2002**, *24* (2), 111–125.

(15) Mattioni, M.; Soddu, S.; Prodosmo, A.; Visca, P.; Conti, S.; Alessandrini, G.; Facciolo, F.; Strigari, L. Prognostic Role of Serum p53 Antibodies in Lung Cancer. *BMC Cancer* **2015**, *15* (1), 1–11.

(16) Nogueira, J. A.; Ono-Nita, S. K.; Nita, M. E.; de Souza, M. M.; do Carmo, E. P.; Mello, E. S.; Scapulatempo, C.; Paranaguá-Vezozzo, D. C.; Carrilho, F. J.; Alves, V. A. 249 TP53 Mutation Has High Prevalence and Is Correlated with Larger and Poorly Differentiated HCC in Brazilian Patients. *BMC Cancer* **2009**, *9* (1), 204.

(17) Fett-Conte, A. C.; Salles, A. B. C. F. A Importância Do Gene p53 na Carcinogênese Humana. *Rev. Bras. Hematol. E Hemoter.* **2002**, *24* (2), 85–89.

(18) Hall, P. A.; Lane, D. P. p53 In Tumour Pathology: Can We Trust Immunohistochemistry?—revisited! *J. Pathol.* **1994**, *172* (1), 1–4.

(19) Campàs, M.; O'Sullivan, C. Layer-by-Layer Biomolecular Assemblies for Enzyme Sensors, Immunosensing, and Nanoarchitectures. *Anal. Lett.* **2003**, *36* (12), 2551–2569.

(20) de la Escosura-Muñiz, A.; Parolo, C.; Merkoçi, A. Immunosensing Using Nanoparticles. *Mater. Today* **2010**, *13* (7–8), 24–34.

(21) Gonzalez, R. C.; Woods, R. E. *Digital Image Processing*, 3rd ed.; Prentice Hall: Upper Saddle River, N.J, 2008.

(22) Shapiro, L. G.; Stockman, G. C. *Computer Vision*; Prentice Hall: Upper Saddle River, NJ, 2001.

(23) Costa, L. da F.; Cesar, R. M.; Costa, L. da F. *Shape Classification and Analysis: Theory and Practice*, 2nd ed.; Image processing series; CRC Press: Boca Raton, 2009.

(24) Ramesan, M. T. Synthesis, Characterization, and Conductivity Studies of Polypyrrole/copper Sulfide Nanocomposites. *J. Appl. Polym. Sci.* **2012**, 1540–1546.

(25) Vishnuvardhan, T. K.; Kulkarni, V. R.; Basavaraja, C.; Raghavendra, S. C. Synthesis, Characterization and A.c. Conductivity of polypyrrole/Y2O3 Composites. *Bull. Mater. Sci.* **2006**, *29* (1), 77–83.

(26) Więckowski, A., Korzeniewski, C., Braunschweig, B. *Vibrational Spectroscopy at Electrified Interfaces*. Wiley: Hoboken, New Jersey, 2013.

(27) Barth, A. The Infrared Absorption of Amino Acid Side Chains. *Prog. Biophys. Mol. Biol.* **2000**, *74* (3–5), 141–173.

(28) Barth, A. Infrared Spectroscopy of Proteins. *Biochim. Biophys. Acta BBA - Bioenerg.* **2007**, *1767* (9), 1073–1101.

(29) Liptay, W. Introduction to Infrared and Raman Spectroscopy. VonN. B. Colthup, L. H. Daly undS. E. Wiberley. Academic Press, New York-London 1964. 1. Aufl., XII, 511 S., zahlr. Abb. u. Tab., geb. £ 12.—. *Angew. Chem.* **1965**, *77* (16), 744–745.

(30) Elif Sen; Gonullu, U.; Akar, N. The Detection of Quantitative Serum Protein in Lung Cancer. *Tuberkulus Ve Toraks Derg.* **2005**, *53*, 231–237.

(31) Silva, O.B.; Machado, S. A. S. Evaluation of the Detection and Quantification Limits in Electroanalysis Using Two Popular Methods: Application in the Case Study of Paraquat Determination. *Anal. Methods* **2012**, *4* (8), 2348–2354.

(32) Arora, S.; Venkataraman, V.; Zhan, A.; Donohue, S.; Biglan, K. M.; Dorsey, E. R.; Little, M. A. Detecting and Monitoring the Symptoms of Parkinson's Disease Using Smartphones: A Pilot Study. *Parkinsonism Relat. Disord.* **2015**, *21* (6), 650–653.

(33) Prasanna, P.; Jain, S.; Bhagat, N.; Madabhushi, A. Decision Support System for Detection of Diabetic Retinopathy Using Smartphones; IEEE, 2013.

(34) Laksanasopin, T.; Guo, T. W.; Nayak, S.; Sridhara, A. A.; Xie, S.; Olowookere, O. O.; Cadinu, P.; Meng, F.; Chee, N. H.; Kim, J.; Chin, C. D.; Munyazesa, E.; Mugwaneza, P.; Rai, A. J.; Mugisha, V.; Castro, A. R.; Steinmiller, D.; Linder, V.; Justman, J. E.; Nsanzimana, S.; Sia, S. K. A Smartphone Dongle for Diagnosis of Infectious Diseases at the Point of Care. *Sci. Transl. Med.* **2015**, *7* (273), 273re1.

Author Contributions Statement

V.C.R. performed experiments and prepared the figures, and wrote the manuscript. C.C. and LdFC performed the image analysis. J.C.S. carried out the QCM measurements and analyzed the corresponding data. A.C.S. performed the PM-IRRAS measurements and analyzed the spectra. M.E.M. and J.H.T.F. performed the extraction and preparation of the cell samples, and measured the biomarker concentration using electrochemiluminescence at the Barretos Cancer Hospital. A.L.C. was responsible for the experiments and data analysis at the Barretos Cancer Hospital. O.N.O was the coordinator of the research, and edited the manuscript. All the authors proofread the manuscript.

Additional Information

Supporting Information. Characterization and control experiments with the biosensor.

Competing financial interests: The authors declare no competing financial interests.

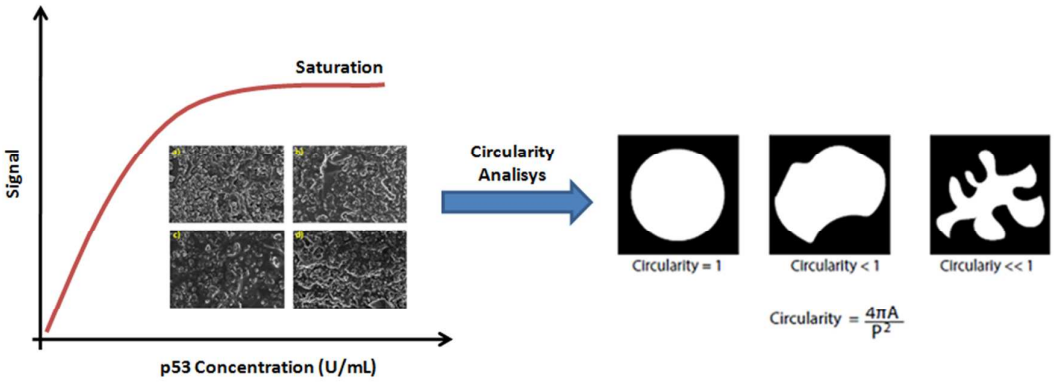

Analysis of Scanning Electron Microscopy Images to Investigate Adsorption Processes Responsible for Detection of Cancer Biomarkers

Valquiria da Cruz Rodrigues[1*], Cesar Comin[1], Juliana Coatrini Soares[1], Andrey Coatrini Soares[1,2], Matias Eliseo Melendez[3], José Humberto T. G. Fregnani[3], André L. Carvalho[3] Luciano da F. Costa[1], Osvaldo N. Oliveira Jr.[1]

Table of Contents

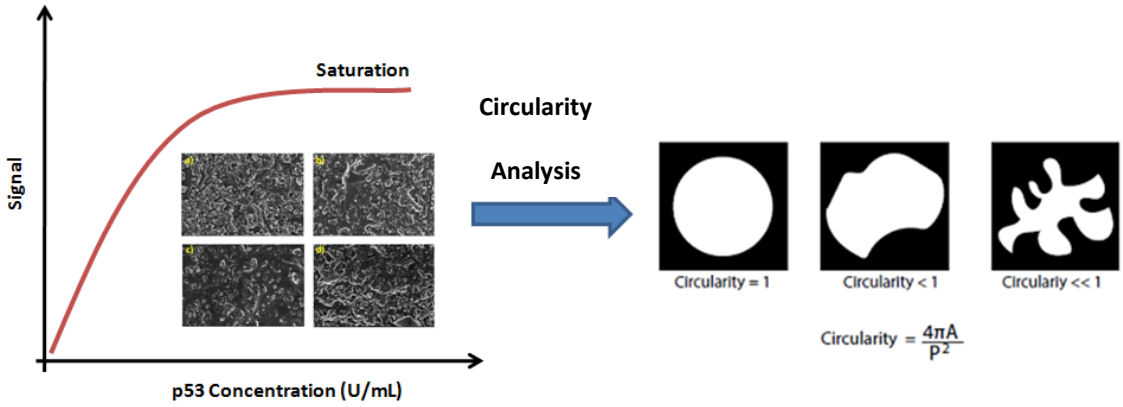

Circularity analysis in SEM images is used to explain adsorption of p-53 biomarker on PPy immunosensor for early detection of head and neck cancer.

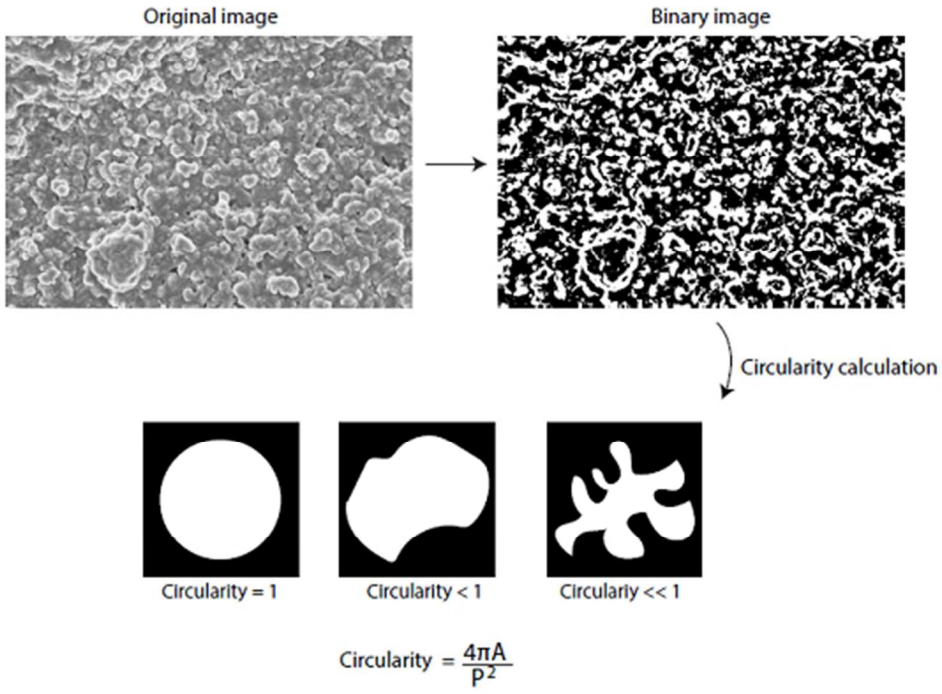

Figure 1: Methodology used for circularity calculation. The original image is transformed into a binary one. The circularity of each white object is then quantified. Objects that are similar to disks have a circularity close to 1, while more irregular objects are represented by smaller circularity values.

150x114mm (96 x 96 DPI)

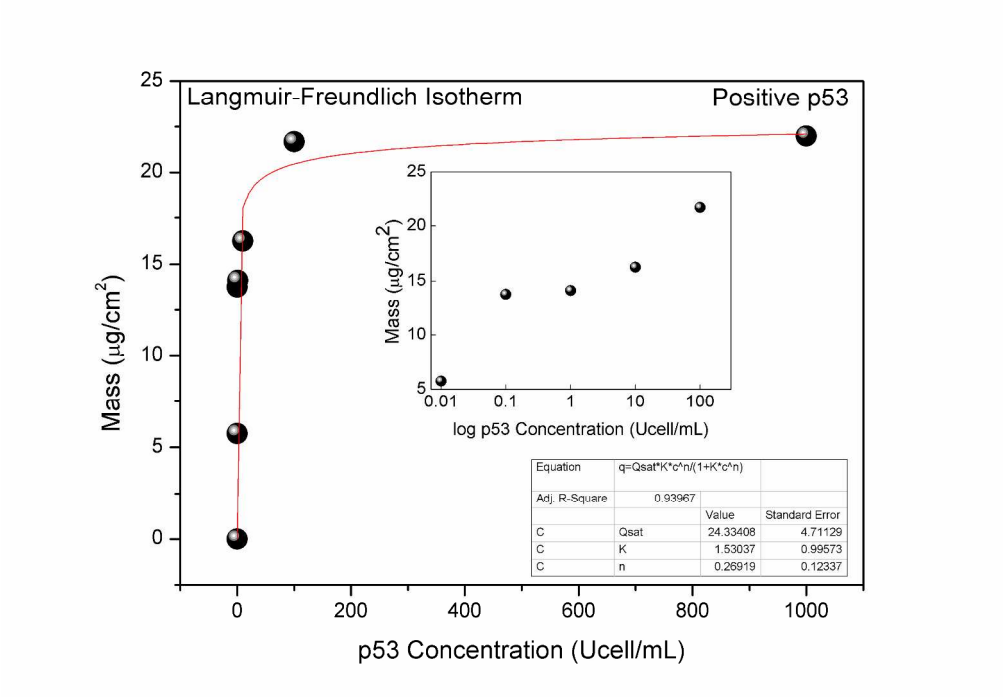

Figure 2. Adsorption isotherm obtained with a QCM, in which the mass adsorbed during the biosensing experiment is plotted against the concentration of p53 antigen. The solid curve shows the fitting with the Langmuir-Freundlich model. The insert shows the data in logarithmic scale

287x201mm (300 x 300 DPI)

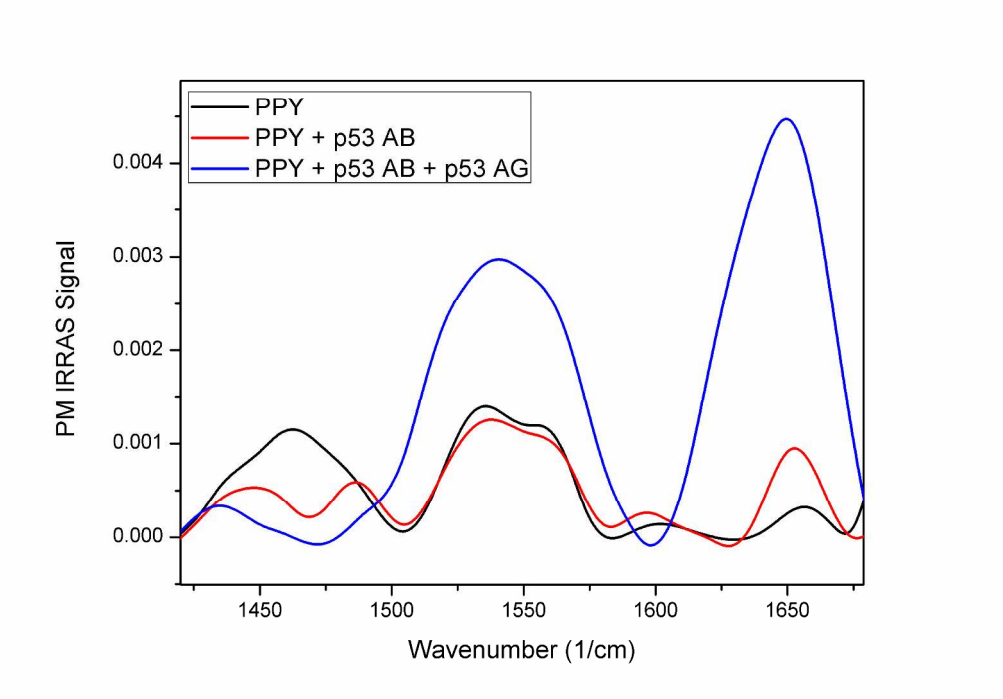

Figure 3. PM-IRRAS spectra of a PPY layer (black), coated with a layer of p53 antibodies (PPY/p53 AB, red) and after adsorption of p53 antigens (PPY/p53 AB/AG, blue). The spectrum of the gold support was used as reference, which was subtracted from the spectra of the films.

287x201mm (300 x 300 DPI)

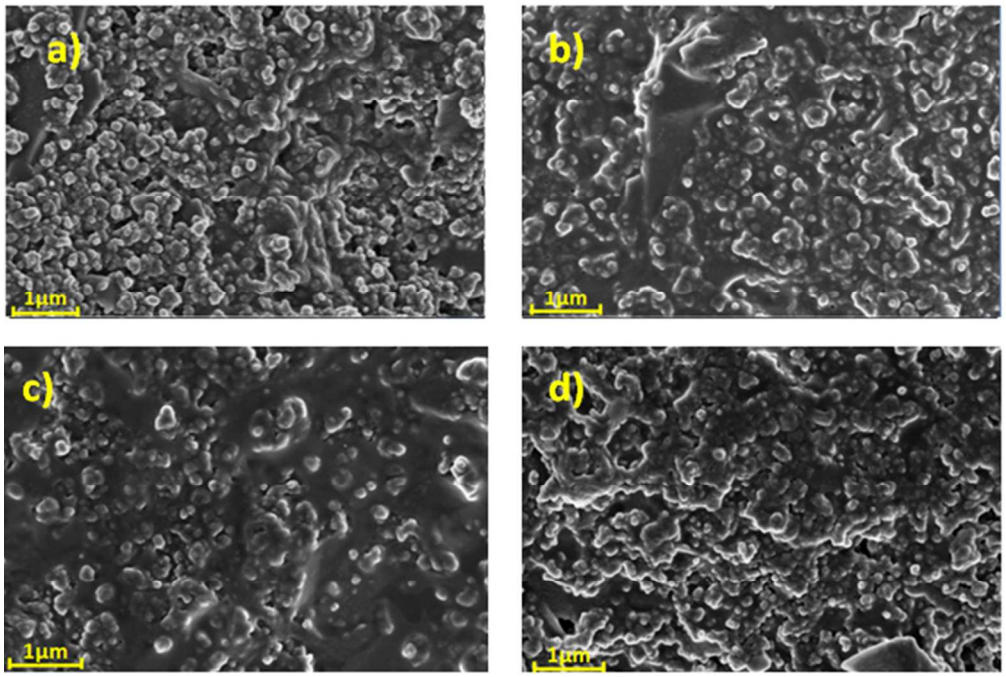

Figure 4. SEM images with increase of 50.000x of films: a) PPy, b) PPy/anti p53, before exposure to the antigen p53, c) PPy/anti p53, after exposure to the antigen p53 and d) PPy/anti p53, after exposure to the antigen p53 at saturation (i.e. very high concentration).

232x156mm (96 x 96 DPI)

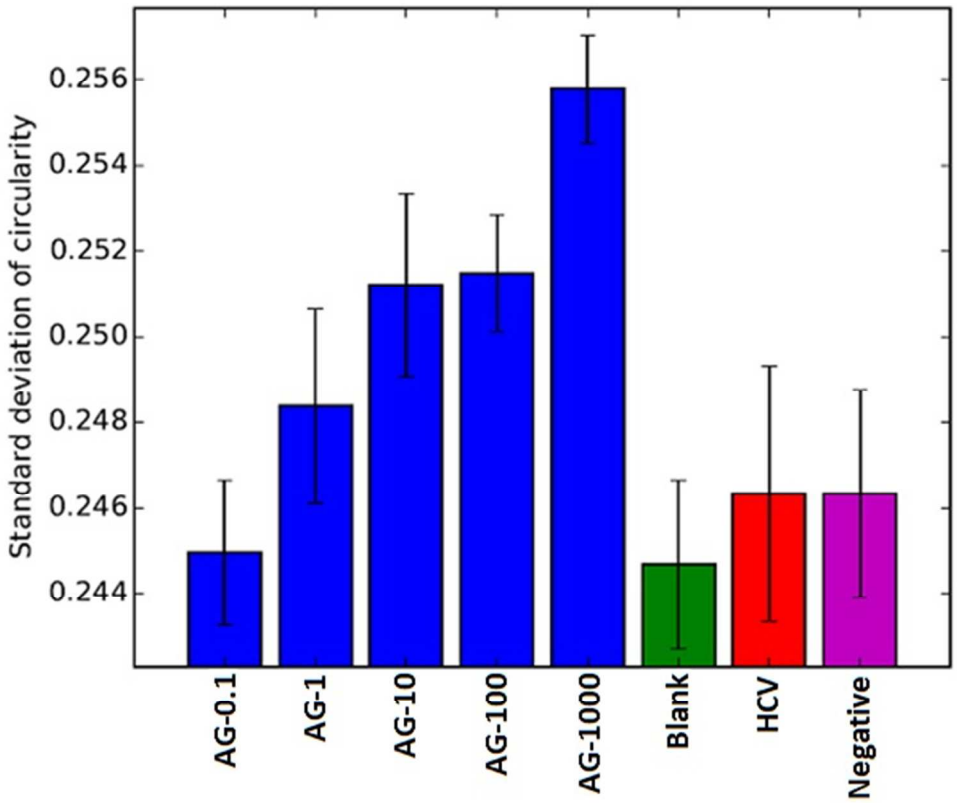

Figure 5. The standard deviation of average circularity obtained in the SEM images varied with the concentration of the antigen p53 to which the biosensor was exposed. Significantly, when non-specific analytes were used, viz. for HCV (red), cells that did not contain p53 (negative, magenta), the standard deviation was very similar to that of the PPy/anti p53 film, before exposure to the antigen p53 (green).

165x136mm (96 x 96 DPI)

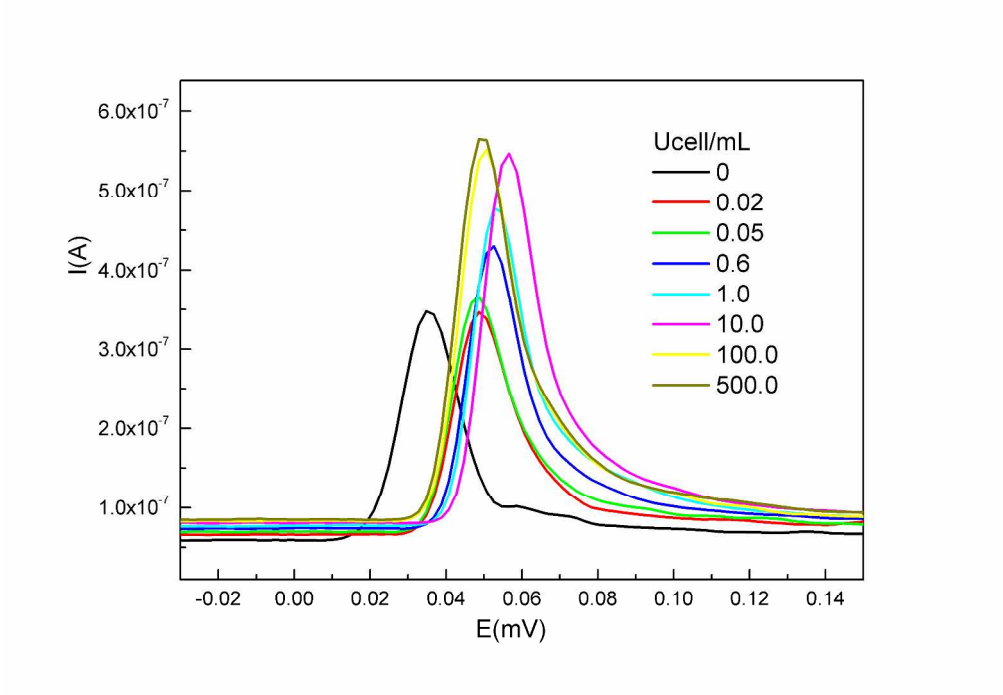

Figure 6. Cyclic voltammetry of PPI/p53 films, in the potential range between -0.6 V and 0.6V vs. SCE in buffer PBS pH 7.4 with p53 antigen ranging between 0 and 500 Ucell/mL.

287x200mm (300 x 300 DPI)

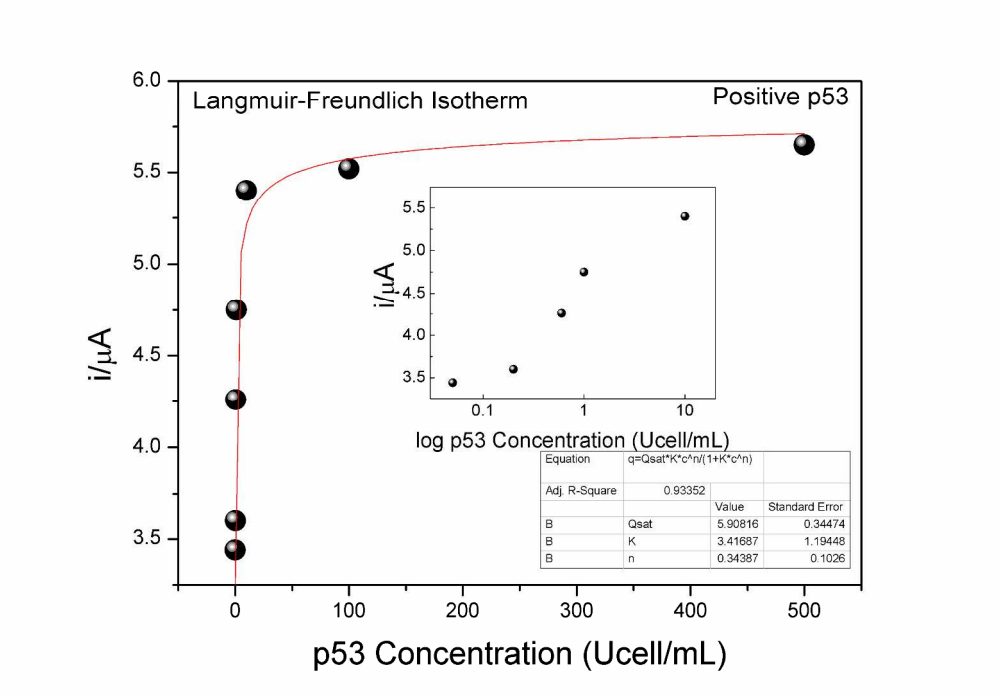

Figure 7. Peak current of cyclic voltammograms for PPY/p53 of Figure 6 for different antigen p53 concentrations.

287x201mm (300 x 300 DPI)